https://doi.org/10.3311/PPee.41621

Periodica Polytechnica Electrical Engineering and Computer Science

Correction of the Stator Flux Demagnetizing Effect at Low Speeds of the Direct Torque Control of Induction Motor

Lazhar Sahraoui[1*], Mohamed Said Nait Said[2]

[1] Electrical and Automatic Engineering Laboratory, Larbi Ben M'hidi University of Oum El Bouaghi, 4001 Ain Beida, P.O.B. 358, Algeria
[2] Higher School of Renewable Energies, Environment and Sustainable Development, Constatin road, 05078 Batna, Algeria
[*] Corresponding author, e-mail: lazhar_sah@yahoo.fr

Received: 16 July 2025, Accepted: 08 January 2026, Published online: 24 February 2026

Abstract

This paper deals with the direct torque control (DTC) of an induction motor. This control allows torque flux to be decoupled without the need for coordinate transformations. It has the advantage of being robust to parametric variations of the machine in tracking mode, and to load disturbances in regulation mode. However, in addition to torque and flux ripples, this control in its conventional version proves insufficient at low speeds due to the demagnetizing effect of the stator flux caused by the ohmic drop across the stator resistor. This demagnetization considerably increases torque and flux ripples and causes current distortions. To alleviate this problem, it is necessary to shift back the flux positions in the (α, β) plane by an appropriate angle. The main objective of this study is to find this offset angle without affecting the entire order in its original version. In speed loop, the parameters of the PI controller are optimized using the Particle Swarm Optimization (PSO) algorithm.

Keywords

direct torque control (DTC), flux demagnetization, stator resistance, induction motor (IM), low speeds

1 Introduction

In view of its simple construction, robustness and easy maintenance, the induction machine is the most frequently used machine in all industrial sectors, particularly in variable-speed drives. On the other hand, his model is non-linear. Torque is strongly coupled to flux. Flux Orientation Control (FOC), introduced in mid-1972, is able to linearize its model, but is sensitive to parametric and non-parametric variations in the machine [1]. Contrary to flux orientation control, direct torque control (DTC) is robust to variations in machine and load parameters. This control offers rapid speed and torque dynamics [2, 3] The DTC introduced by Depenbrock [4], and Takahashi and Kanmachi [5] is based on the torque imposed on the machine and the maintenance of the stator flux at its reference value through direct action on the state of the converter switches. Depending on the position of the flux in the (α, β) plane, in one of its six positions, a selection table is used to choose the voltage vector to be applied. At each sampling instant, the flux is calculated by neglecting the stator resistance, which is not valid for low speeds, as this causes demagnetization. This demagnetization is due to the voltage drop across the stator resistor. The flux is nowhere near its reference value, causing torque and current ripples. To compensate for this demagnetization, research has been carried out to improve control at low speeds, while retaining the full functionality of the DTC in its classic version, without resorting to more complex techniques [2, 6, 7].

2 Motor and converter vector models

The model of the machine in reference frame (α, β) in dynamic regime is expressed by [8, 9]:

$$\bar{v}_s = R_s \bar{i}_s + \frac{\bar{\phi}_s}{dt}, \tag{1}$$

$$\bar{v}_r = R_r \bar{i}_r + \frac{\bar{\phi}_r}{dt} - j\omega\bar{\phi}_r, \tag{2}$$

$$\bar{\phi}_s = L_s \bar{i}_s + M\bar{i}_r, \tag{3}$$

$$T_e = k\phi_s\phi_r \sin\delta, \tag{4}$$

By solving the system of Eqs. (3) and (4), we obtain:

$$\bar{i}_s = \frac{1}{\sigma L_s}\bar{\phi}_s - \frac{M}{\sigma L_s L_r}\bar{\phi}_r, \tag{5}$$

Cite this article as: Sahraoui, L., Nait Said, M. S. "Correction of the Stator Flux Demagnetizing Effect at Low Speeds of the Direct Torque Control of Induction Motor", Periodica Polytechnica Electrical Engineering and Computer Science, 2026. https://doi.org/10.3311/PPee.41621

$$\bar{i}_r = \frac{1}{\sigma L_r}\bar{\phi}_r - \frac{M}{\sigma L_s L_r}\bar{\phi}_s, \tag{6}$$

$$T_e = k\phi_s\phi_r \sin\delta, \tag{7}$$

with:

$$k = p\frac{1}{L_s L_r} \text{ and } \delta = \left(\widehat{\bar{\phi}_s, \bar{\phi}_r}\right),$$

and the equation mechanic:

$$T_e - T_r = \frac{d\Omega}{dt} + f\Omega, \tag{8}$$

with:

$$\omega = p\Omega.$$

The voltage vector is delivered by a three-phase voltage inverter whose two switches on the same arm operate in complementarily. These switches are controlled by 3 Boolean control quantities S_a, S_b, S_c. The voltage vector is thus written:

$$\bar{V}_s = \sqrt{2/3}E\left(S_a + S_b e^{j\frac{2\Pi}{3}} + S_c e^{j\frac{4\Pi}{3}}\right). \tag{9}$$

The combinations of the three quantities generate 8 positions of the vector $\bar{V}_s$ two of which are zero vectors $(\bar{V}_0, \bar{V}_7)$ as shown in Fig. 1.

3 Direct torque control (DTC)

3.1 Structure control

The principle of direct torque control is based on the selection of an appropriate sequence of inverter control switches,

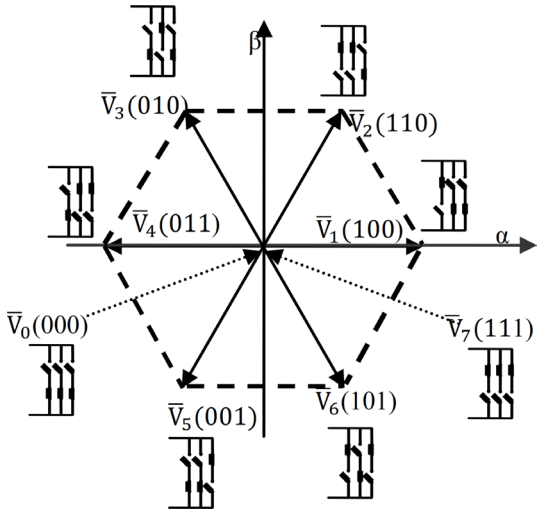

Fig. 1 Voltage vector evolution in space

which allows both stator and rotor fluxes to be maintained at their references, and torque to be modified according to its set value [10]. The control structure is presented in Fig. 2.

3.2 Flux control

Flux is estimated using Eq. (1) by measuring the stator current and voltage and estimating the stator resistance R_s. The integration during the application time T_c of a vector $\boldsymbol{V_s} = V_{si}$ between the two instants t_k and $t_{k+1} = t_k + T_c$:

$$\int_{\bar{\phi}_{s(k)}}^{\bar{\phi}_{s(k+1)}} d\bar{\phi}_s = \int_{t_k}^{t_{k+1}} \left(\bar{V}_s dt - R_s \bar{i}_s\right) dt. \tag{10}$$

At high speeds, the voltage drop across the stator resistor is negligible compared to the voltage applied to the machine, and the flux has the following expression:

$$\bar{\phi}_s(k+1) - \bar{\phi}_s(k) = \bar{V}_{si} T_c. \tag{11}$$

The end of the flux vector moves along a straight line in the direction of the vector $\boldsymbol{V_s}$ as shown in Fig. 3 and its displacement velocity is giiven by

Its displacement velocity is given by:

$$d\bar{\phi}_s / dt = \bar{V}_s = \sqrt{2/3}E.$$

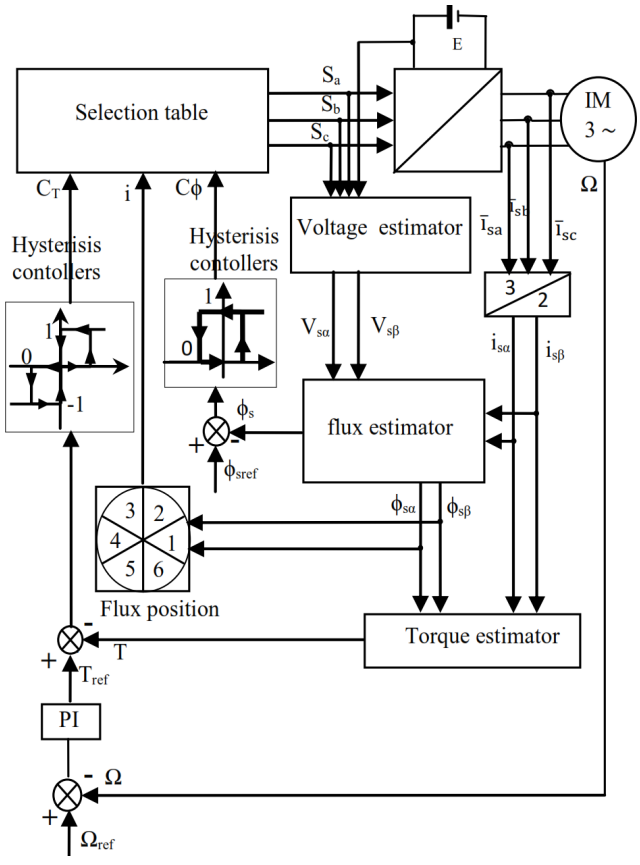

Fig. 2 Direct torque control structure

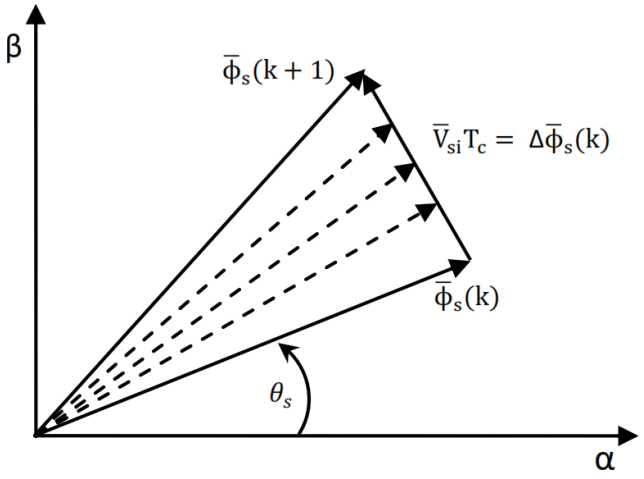

Fig. 3 Stator flux in reference frame (α, β)

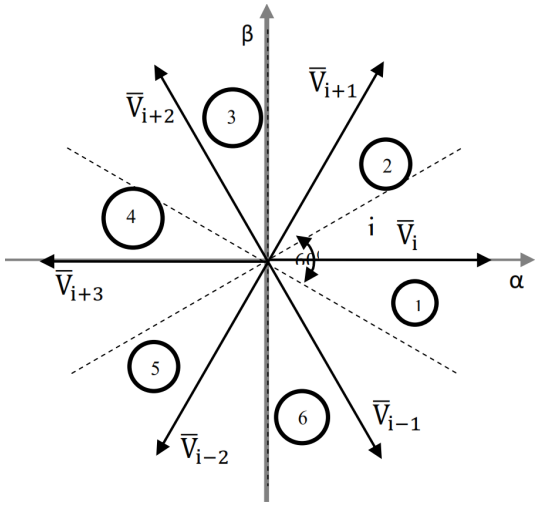

Fig. 4 Choice of vector $\bar{V}_s$

3.3 Torque control

By applying a suitable voltage vector sequence for a time Δt, the stator flux retains its modulus and its rotational speed is increased or decreased by a pulsation value $\Delta\omega_s$, while the rotor flux retains its modulus and rotational speed. This variation in position between the two fluxes is given by Eq. (11):

$$\Delta\delta = \Delta\omega_s \Delta t. \tag{12}$$

Referring to Eq. (11), the torque is written:

$$T_e = k\phi_s\phi_r \sin\left(\delta_0 + \Delta\delta\right). \tag{13}$$

Torque increases or decreases as stator flux accelerates or decelerates [11].

3.4 Choice of vector

The choice of the vector $\bar{V}_s$ depends on the position of the stator flux vector $\bar{\phi}_s$ in the reference frame (α, β) and the desired variation in torque and flux, as well as the direction of rotation of ω_s.

Indeed, the stator flux evolution space $\bar{\phi}_s$ in reference frame (α, β) is divided in six zones i = 1 to 6 as shown in Fig. 4. If flux $\bar{\phi}_s$ is in zone i, flux and torque control is ensured by selecting one of these six following voltage vectors, if:

- $\bar{V}_{i+1}$ is selected, the magnitude of the flux increases and undergoes an acceleration, resulting in an increase in torque.
- $\bar{V}_{i-1}$ is selected, the magnitude of the flux increases and undergoes a deceleration, leading to a decrease in torque.
- $\bar{V}_{i+2}$ is selected, the magnitude of the flux decreases and undergoes an acceleration, hence the increase in torque.
- $\bar{V}_{i-2}$ is selected, the magnitude of the flux decreases and undergoes a deceleration, hence the decrease in torque.
- $\bar{V}_0$ and $\bar{V}_7$ are selected, the magnitude of the flux remains constant and stops rotating, hence the decrease in torque.
- The vectors $\bar{V}_i$ and $\bar{V}_{i+3}$ are never selected.
- The effect of the selected voltage vectors depends on the position of the flux $\bar{\phi}_s$ within zone i.

At the beginning of the zone, the voltage vectors $\bar{V}_{i+1}$ and $\bar{V}_{i-2}$ are perpendicular to the flux $\bar{\phi}_s$ and cause it to vary slowly, while the torque undergoes a rapid change. At the end of the zone, the effect is reversed.

The voltage vectors $\bar{V}_{i+2}$ and $\bar{V}_{i-1}$ are perpendicular to the flux $\bar{\phi}_s$ at the end of the zone and cause it to vary rapidly, while the torque changes slowly. At the beginning of the zone, the effect is reversed.

Regardless of the direction of flux and torque evolution within zone i, the vectors $\bar{V}_i$ and $\bar{V}_{i+3}$ are never selected because they rapidly increase the flux magnitude to its maximum. However, their effect on the torque depends on the position of the flux within zone i, where the effect is null at the middle of the zone.

4 Selection table

The selection table is built according to the binary variables of the two controllers and the stator flux position in zone i (Table 1) [12].

5 Low-speed direct torque control

If we disregard the resistance R_s, the end of the stator flux $\bar{\phi}_s$ is held practically by the control in a circular ring. This

Table 1 Selection table

C_ϕ		1			0	
C_T	1	0	−1	1	0	−1
1	$\bar{V}_2$	$\bar{V}_7$	$\bar{V}_6$	$\bar{V}_3$	$\bar{V}_0$	$\bar{V}_5$
2	$\bar{V}_3$	$\bar{V}_0$	$\bar{V}_1$	$\bar{V}_4$	$\bar{V}_7$	$\bar{V}_6$
3	$\bar{V}_4$	$\bar{V}_7$	$\bar{V}_2$	$\bar{V}_5$	$\bar{V}_0$	$\bar{V}_1$
4	$\bar{V}_5$	$\bar{V}_0$	$\bar{V}_3$	$\bar{V}_6$	$\bar{V}_7$	$\bar{V}_2$
5	$\bar{V}_6$	$\bar{V}_7$	$\bar{V}_4$	$\bar{V}_1$	$\bar{V}_0$	$\bar{V}_3$
6	$\bar{V}_1$	$\bar{V}_0$	$\bar{V}_5$	$\bar{V}_2$	$\bar{V}_7$	$\bar{V}_4$

is not valid at low speeds and during start-up, as the voltage drop across this resistor alters the evolution of the end of flux $\bar{\phi}_s$. In fact, calculating the flux while taking into account the voltage drop across the resistor R_s modifies the evolution of the end of the flux by deviating from its theoretical trajectory and follows that of the electromotive force $\bar{e}_s$ which in advance on the voltage as shown in Fig. 5 [13].

As an example, at the beginning of the zone (i = 1), the flux does not follow the direction of the voltage $\bar{V}_2$ that is applied to increase its modulus. The end of the flow deviates from the circle and undergoes a slight decay which requires selection of the vector $\bar{V}_2$ over several sampling periods. This phenomenon acts on the currents in the stator phases, affecting their orientation and modifying their modulus, leading to their deformation and inevitably to torque ripple. In fact, current is expressed as:

$$\bar{i}_s = \frac{1}{\sigma Ls}\bar{\phi}_s - \frac{M}{\sigma L_s L_r}\bar{\phi}_r. \tag{14}$$

The rotor flux $\bar{\phi}_r$ is not affected by this phenomenon, resulting in the direct impact of the stator flux $\bar{\phi}_s$ on the current $\bar{i}_s$.

These effects can be corrected by shifting the stator flux zones backwards, while maintaining Table 1 unchanged. In this case, the voltage vector $\bar{V}_1$ is selected, providing effective flux control [14, 15].

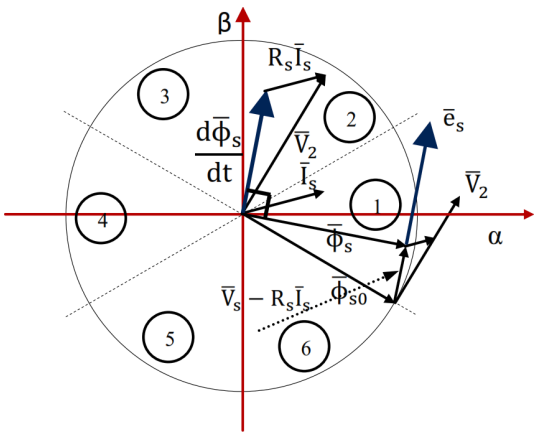

Fig. 5 Stator flux at low speed in reference frame (α, β)

In speed loop, the parameters of the PI controller are initially calculated using pole placement and then optimized using the Particle Swarm Optimization (PSO) algorithm.

This algorithm, proposed by Kennedy and Eberhart [15], is inspired by the collective behavior observed in flocking birds and schooling fish.

Particle Swarm Optimization (PSO) is a stochastic, self-adaptive, population-based optimization method inspired by the collective behavior observed in natural swarms. The algorithm begins by generating an initial set of N particles, each characterized by a position $x_i(k)$ and a velocity $v_i(k)$ at iteration step k.

At each iteration, the objective function is evaluated at the current position of every particle, allowing the identification of the individual best position $p_i(k)$ (p_{best}) and the global best position $g(k)$ (g_{best}) discovered by the swarm up to that point.

The dynamics of the swarm are governed by the standard PSO update equations:

$$\begin{aligned} V_i(k+1) &= \omega V_i(k) + C_1 r_1 \left(p_i - X_i(k)\right) \\ &+ C_2 r_2 \left(g(k) - X_i(k)\right), \end{aligned} \tag{15}$$

$$X_i(k+1) = X_i(k) + V_i(k+1), \tag{16}$$

where ω denotes the inertia weight, C_1 and C_2 represent the cognitive and social acceleration coefficients, and r_1 and r_2 are random variables uniformly distributed over [0, 1]. To ensure that the particles remain within the valid search space.

Bound constraints are imposed on particle positions and velocities to ensure that they remain within the predefined search domain:

$$X_{\min} < X_i(k) < X_{\max} \text{ and } V_{\min} < V_i(k) < X_{\max}.$$

In the present study, the cost function is defined as:

$$C = \int_0^t \left|\Omega_{ref}(\tau) - \Omega(\tau)\right| d\tau, \tag{17}$$

where Ω_{ref} denotes the reference speed and Ω the actual motor speed. This function is specifically designed to minimize the tracking error over time, thereby improving the dynamic performance of the system. The PSO algorithm was executed for a total of $k_{\max}$ iterations, used here as the stopping criterion [15, 16].

The optimal controlling parameters of the classical and proposed optimal PI controller are shown in Table 2 at the end of the test period.

The convergence process of the proposed algorithm is demonstrated in Fig. 6, and the optimized PI parameters are obtained after 90 iterations (see Table 3).

Table 2 Main parameters of the PSO algorithm

Name	Symbol	Value
Swarm size	N	50
Inertia weight	ω	0.7
Cognitive coefficient	C_1	1.5
Social coefficient	C_2	1.5
Maximum iterations	k_{max}	120

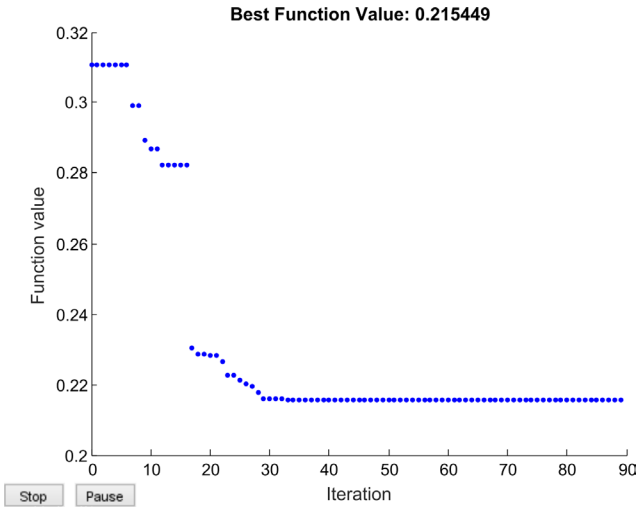

Fig. 6 Iteration curves for PSO algorithm

Table 3 Optimized PI parameters

Tuning method	K_p	K_i
Pole placement	23.7390	107.811
PSO	20.7248	471.500

6 Simulation results

In Simulink in a MATLAB [17] environment, simulation tests were carried out on the machine under the following conditions:

$$\phi_{ref} = 1.00 \text{ Wb}, \ \Delta\phi = \pm 0.01 \text{ Wb}, \ \Delta T_r = \pm 2.5 \text{ Nm},$$
$$T_r = T_{rN} = 50 \text{ Nm}, \ \Omega_{ref} = 20 \text{ rad/s},$$

where:

- ϕ_{ref}: reference stator flux;
- $\Delta\phi$: regulator stator flux band;
- ΔT_r: regulator load torque band;
- T_r: load torque;
- Ω_{ref}: reference rotor speed.

The machine to be simulated is shown in Table 4.

The simulation is carried out in three steps:

- This first step involves carrying out a simulation of the classic DTC with and without a control loop.
- In the second step, the simulation is carried out on the DTC in the zone shifted by $\theta_d = \pi/12$ with and without the control loop. This shift angle θ_d is the result of a series of simulation tests such that $(0 < \theta_d < \pi/6)$.
- The last step is to carry out robustness tests.

Table 4 Machine rating plate and parameters

Name	Values
Nominal power (P_N)	7.5 kW
Pairs poles number (p)	2
Frequency (f)	50 Hz
Nominal speed (Ω_N)	150 rad/s
Nominal tension (U_s)	220/380 V
R_s	0.63 Ω
R_r	0.40 Ω
L_s	0.097 H
L_r	0.091 H
M	0.091 H
J	0.22 kg M^2
B	0 SI

The shift of the stator flux vector is clearly illustrated in Fig. 7 by the presentation of the instantaneous flux along the alpha axis.

Indeed, as shown in Fig. 8, the stator flux standard quickly returns to its reference after correction. The stator flux standard reaches its reference after 0.06 s after correction, but without correction, it reaches its reference after almost 0.12 s. This is equivalent to a 50% gain. We can therefore say that the stator flux offset, which constitutes the low-speed control correction, has been successful in terms of the time taken for the flux to stabilize at its reference.

With regard to current, it is interesting to note, as shown in Fig. 9, that after correction, the stator current approaches a sinusoidal waveform, whereas before correction, the current exhibits distortions. The closed-loop speed and torque, as shown in Figs. 10 and 11, are not significantly affected by the correction, except that it should be noted that at the start

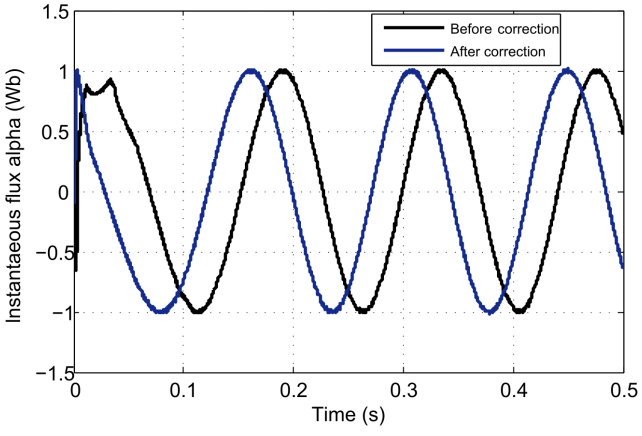

Fig. 7 Instantaneous flux alpha evolution in closed-loop

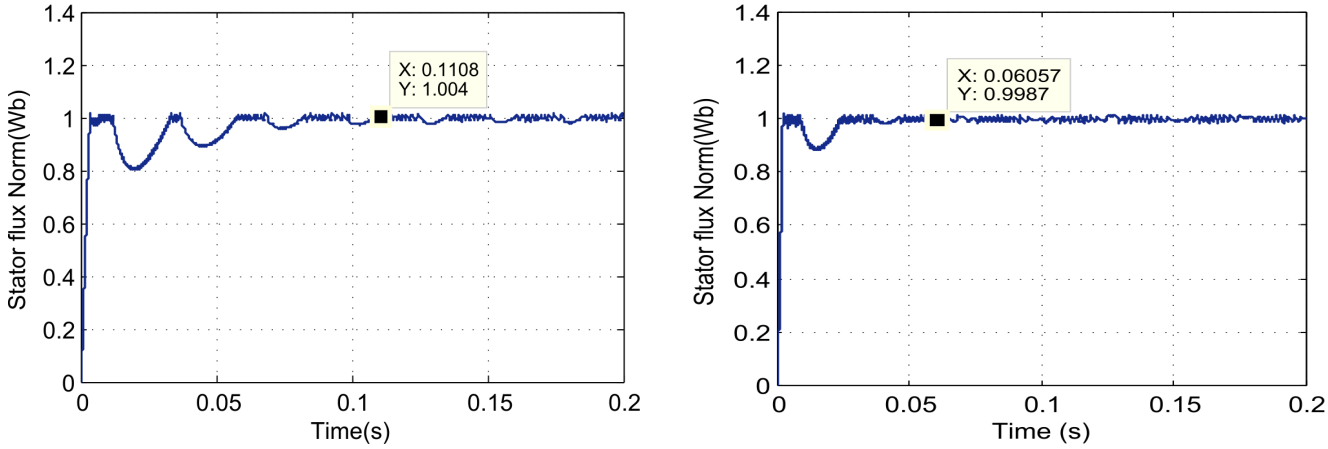

(a) (b)

Fig. 8 Stator norm flux evolution in closed-loop: (a) Before correction; (b) After correction

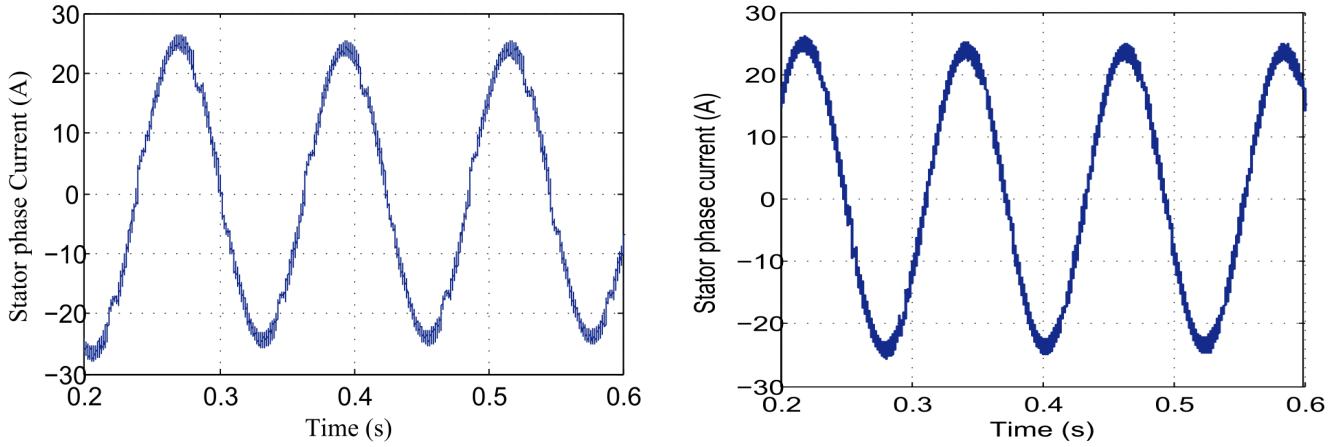

(a) (b)

Fig. 9 Stator phase current evolution in closed-loop: (a) Before correction; (b) After correction

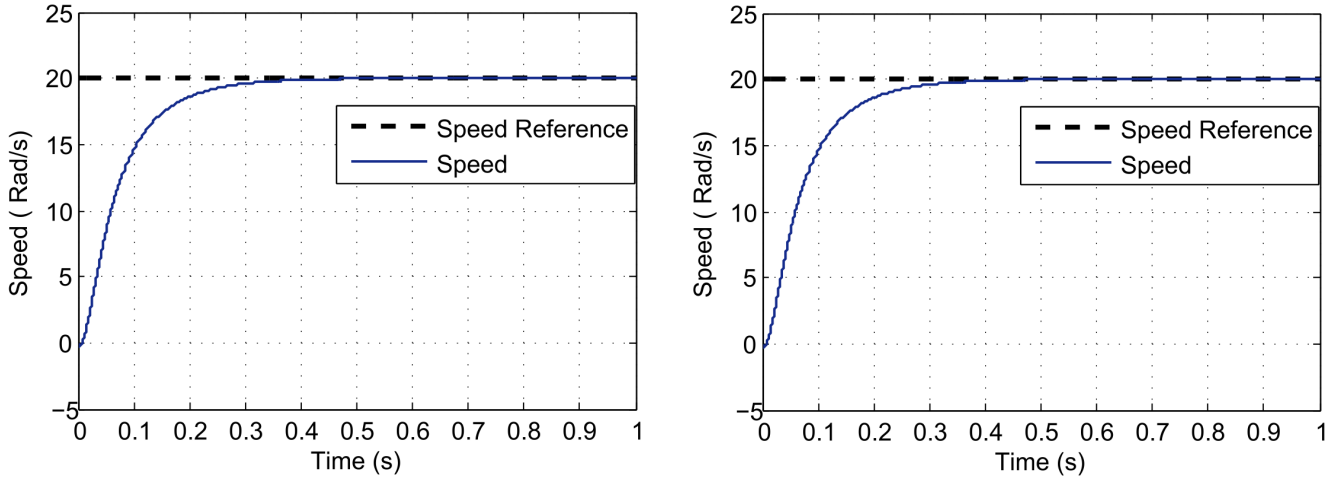

(a) (b)

Fig. 10 Speed evolution in closed-loop: (a) Before correction; (b) After correction

of the start-up, the load attempted to drive the motor, which quickly resumed its role thanks to the good performance of the controllers. However, in open loop, Fig. 12 clearly shows that the improvement in torque ripple. This represents 5.96% compared to the reference torque, whereas before the correction the rate was 8.5%.

The correction has indeed brought a clear improvement in the rapid convergence of the stator flux within its circular trajectory, as shown in Fig. 13.

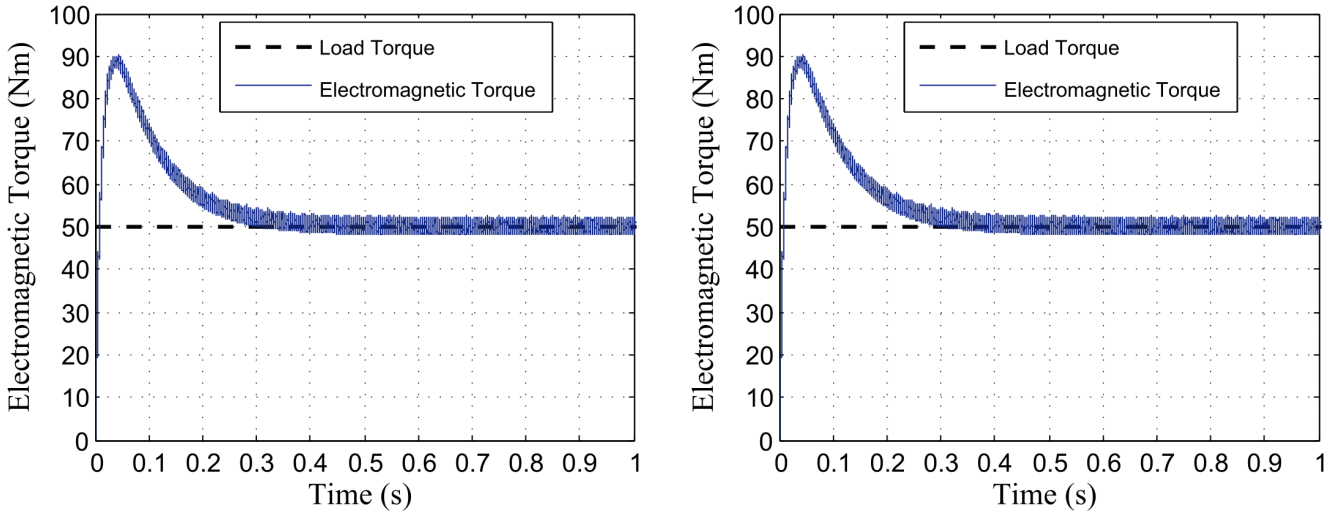

(a) (b)

Fig. 11 Torque evolution in closed-loop: (a) Before correction; (b) After correction

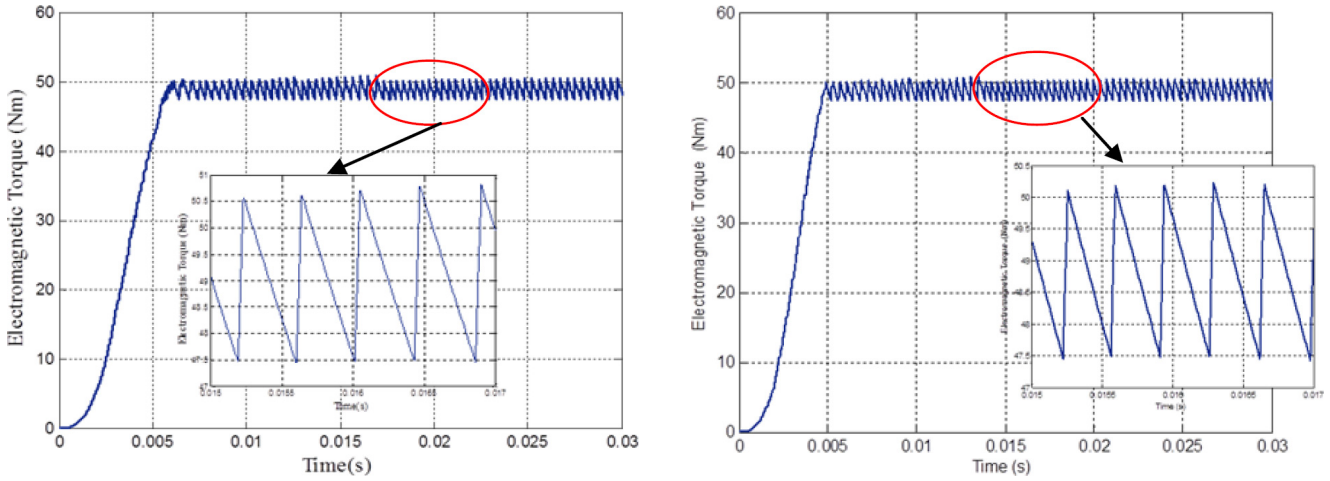

(a) (b)

Fig. 12 Torque electromagnetic evolution in open-loop: (a) Before correction; (b) After correction

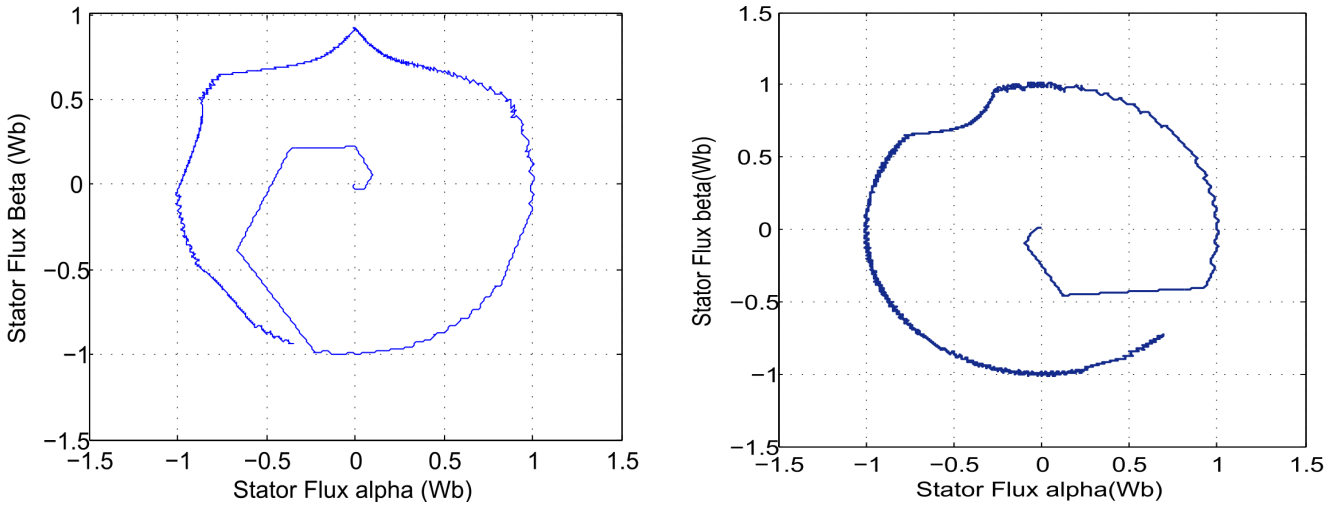

(a) (b)

Fig. 13 Stator flux evolution in (α, β) reference frame in open-loop: (a) Before correction; (b) After correction

Applying this low-speed correction, also known as the shifted zones method, robustness tests with respect to parametric and non-parametric variations were conducted.

A speed reversal test was carried out in closed-loop mode, clearly demonstrating normal two-quadrant operation, as shown in Fig. 14 (a).

A second test involving variation of the rotor resistance clearly shows that the direct torque control at low speeds, after correction, is effective, as illustrated in Fig. 15.

For the load variation test, which is considered a non-parametric variation, it is very clear, as shown in Fig. 16, that at the moment of the load torque change, the speed experiences a slight drop due to its increase. However, this drop lasts only a few seconds, and the speed quickly returns to stability, which demonstrates the good performance of this control strategy.

For all open-loop simulations, a filter was inserted after the speed reference in order to smooth it.

The stator flux does not depend on the variation of the load torque, which explains that the latter is decoupled from the flux. As a result, the system model including the machine and the control becomes linearized.

7 Conclusion

Conventional direct torque control at low speeds leads to flux demagnetization due to the voltage drop across the stator resistor, which affects control performance. To correct this demagnetization, an alternative is to shift the flux zones to the back at an appropriate angle. This shift in flux has given good results.

As a result, flux dynamics have improved considerably, and flux, torque and current ripples have improved. In addition, the machine model is linear zed and there is perfect decoupling between flux and torque.

This flux shifting method is simple, unlike other complex methods such as fuzzy logic and neural networks.

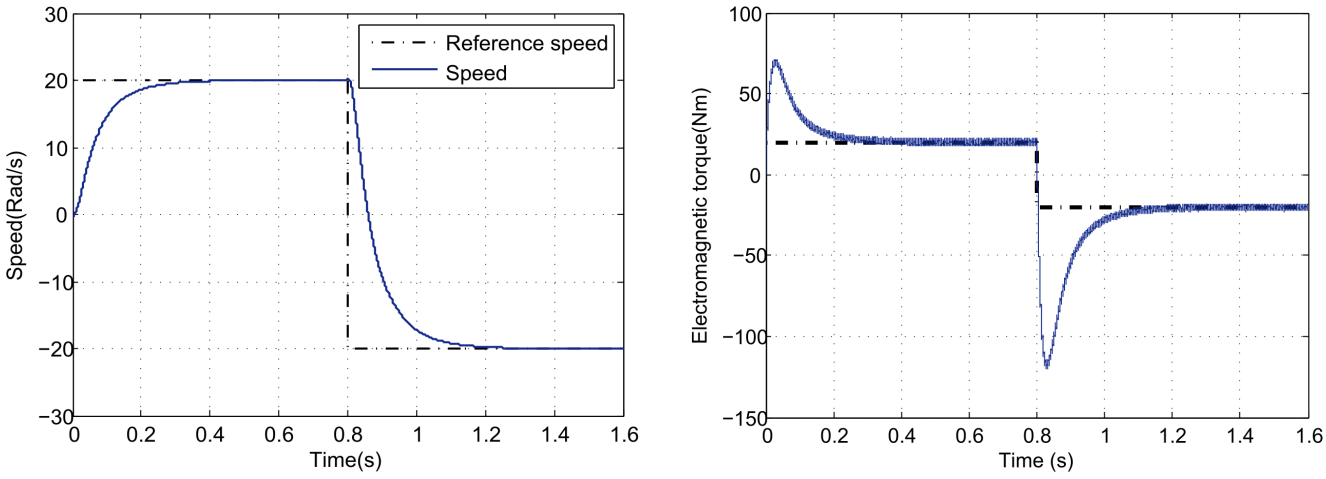

(a) (b)

Fig. 14 Speed inversion test: (a) Evolution speed; (b) Evolution torque

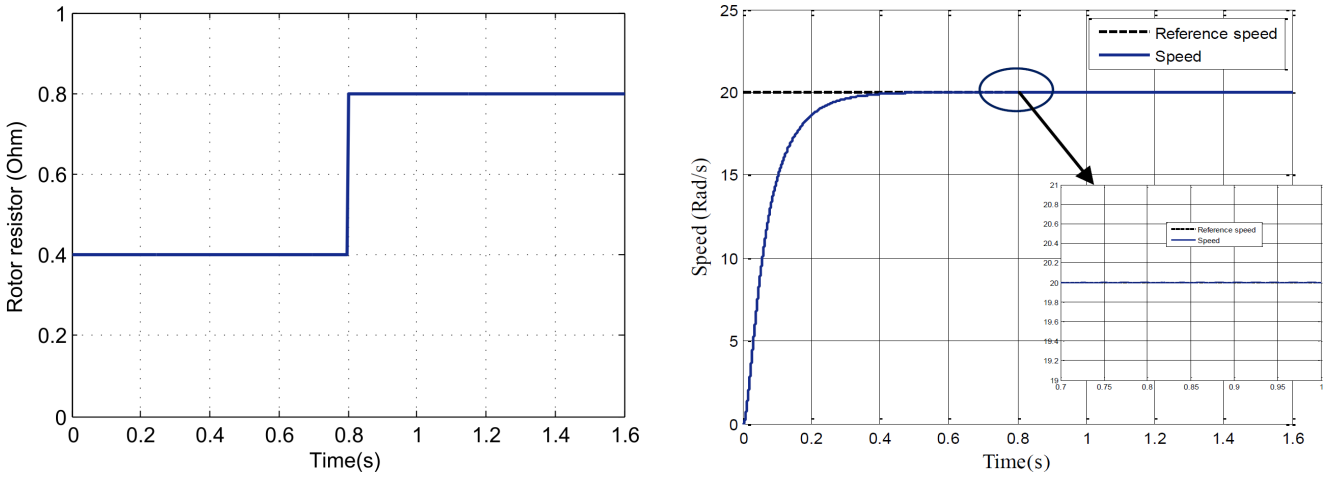

(a) (b)

Fig. 15 Robustness test with respect to rotor resistance variation: (a) Evolution rotor resistor; (b) Evolution speed

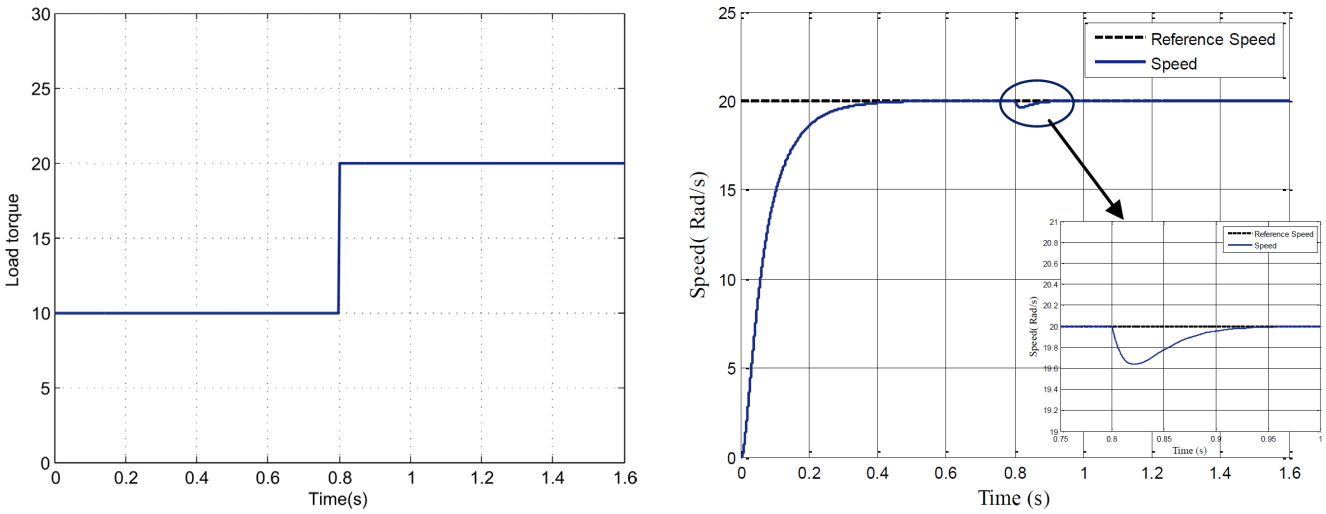

(a) (b)

Fig. 16 Robustness test with respect to load torque variation: (a) Evolution load torque; (b) Evolution speed

In the future, this work can be completed by another equally simple method, shifting the flux zones by −30°, which leads to direct control of the modified torque while modifying Table 1. It is also possible to divide the flow space into twelve sectors and modify Table 1 accordingly.

Nomenclature

R_s: stator resistance
R_r: rotor resistance
L_s, L_r, M: self and mutual inductances
ω: rotor pulsation
Ω: rotor speed
p: number of pole pairs
E: rectified voltage applied to the inverter
T_e: electromagnetic torque
T_r: load torque
$\bar{v}_s, \bar{v}_r$: stator, rotor voltages in frame (α, β)
$\bar{i}_s, \bar{i}_r$: stator, rotor currents in frame (α, β)
$\bar{\phi}_s, \bar{\phi}_r$: stator, rotor flux in frame (α, β)
f: friction coefficient
J: inertia moment
C_T: torque controller binary value
C_ϕ: flux controller binary value

References

[1] Blaschke, F., Siemens AG, Siemens Corp. "Apparatus for field-oriented control or regulation of asynchronous machines", Munich, Germany, US3805135A (Expired - Lifetime), 1971. [online] Available at: https://patents.google.com/patent/US3805135A [Accessed: 05 January 2026]

[2] Mencou, S., Ben Yakhlef, M., Tazi, E. B. "Advanced Torque and Speed Control Techniques for Induction Motor Drives: A Review", In: 2022 2nd International Conference on Innovative Research in Applied Science, Engineering and Technology (IRASET), Meknes, Morocco, 2022, pp. 1–9. ISBN 978-1-6654-2209-3 https://doi.org/10.1109/IRASET52964.2022.9738368

[3] El Ouanjli, N., Derouich, A., El Ghzizal, A., Chebabhi, A., Taoussi, M. "A comparative study between FOC and DTC control of the Doubly Fed Induction Motor (DFIM)", In: 2017 International Conference on Electrical and Information Technologies (ICEIT), Rabat, Morocco, 2017, pp. 1–6. ISBN 978-1-5386-1516-4 https://doi.org/10.1109/EITech.2017.8255302

[4] Depenbrock, M. "Direct self-control (DSC) of inverter-fed induction machine", IEEE Transactions on Power Electronics, 3(4), pp. 420–429, 1988. https://doi.org/10.1109/63.17963

[5] Takahashi, I., Kanmachi, T. "Ultra-wide speed control with a quick torque response AC servo by a DSP", In: 4th European Conference on Power Electronics and Applications, Florence, Italy, 1991, 572.

[6] Belaid, S. L. "Improved IM DTC by using a Fuzzy Switching Table in PV Applications", Elektrotehniški Vestnik, 88(1–2), pp. 26–32, 2021. [online] Available at: https://ev.fe.uni-lj.si/1-2-2021/Belaid.pdf [Accessed: 05 January 2026]

[7] Lazreg, M. H., Bentaallah, A., Mesai-Ahmed, H., Djeriri, Y. "An improved artificial neural network for a direct-power control based on instantaneous power-ripple minimization of the shunt active-power filter", Elektrotehniški Vestnik, 89(4), pp. 181–187, 2022. [online] Available at: https://ev.fe.uni-lj.si/4-2022/Lazreg.pdf [Accessed: 05 January 2026]

[8] Sutikno, T., Idris, N. R. N., Jidin, A. "A review of direct torque control of induction motors for sustainable reliability and energy efficient drives", Renewable and Sustainable Energy Reviews, 32, pp. 548–558, 2014. https://doi.org/10.1016/j.rser.2014.01.040

[9] Caron, J.-P., Hautier, J. P. "Modélisation et Commande de la Machine Asynchrone" (Modeling and Control of the Asynchronous Machine), Éditions Technip, 1995. ISBN 9782710806837 (in French)

[10] Le, T.-L., Hsieh, M.-F. "An enhanced direct torque control strategy with composite controller for permanent magnet synchronous motor", Asian Journal of Control, 26(4), pp. 1683–1702, 2024. https://doi.org/10.1002/asjc.3306

[11] Takahashi, I., Noguchi, T. "A New Quick-Response and High-Efficiency Control Strategy of an Induction Motor", IEEE Transactions on Industry Applications, IA-22(5), pp. 820–827, 1986. https://doi.org/10.1109/TIA.1986.4504799

[12] Gdaim, S., Mtibaa, A., Mimouni, M. F. "Direct Torque Control of Induction Machine based on Intelligent Techniques", International Journal of Computer Applications, 10(8), pp. 29–35, 2010. https://doi.org/10.5120/1500-2017

[13] Chapuis, Y. A., Roye, D., Courtine, S. "Commande directe du couple d'une machine asynchrone par le contrôle direct de son flux statorique" (Direct torque control of an asynchronous machine by direct control of its stator flux), Journal de Physique III, 5(6), pp. 863–880, 1995. (in French) https://doi.org/10.1051/jp3:1995165

[14] Sabri, N. S. M., Tarusan, S. A. A., Zawawi, S. A. S. A., Jidin, A., Sutikno, T. "Optimizing low-speed DTC performance for three-phase induction motors with sector rotation strategy", International Journal of Power Electronics and Drive Systems (IJPEDS), 16(1), pp. 464–471, 2025. https://doi.org/10.11591/ijpeds.v16.i1.pp464-471

[15] Kennedy, J., Eberhart, R. "Particle swarm optimization", In: Proceedings of ICNN'95 - International Conference on Neural Networks, Perth, WA, Australia, 1995, pp. 1942–1948. ISBN 0-7803-2768-3 https://doi.org/10.1109/ICNN.1995.488968

[16] Vinh, N. Q., Le, T.-L. "Self-learning model-based control for sensorless induction motor drives", Electrical Engineering, 107(9), pp. 12169–12182, 2025. https://doi.org/10.1007/s00202-025-03146-z

[17] The MathWorks, Inc. "MATLAB, (R2013a)", [computer program] Available at: https://www.mathworks.com/products/matlab.html [Accessed: 12 July 2025]